Aust. Met. Mag. 39 (1991) 211–222

The Darwin Area Forecasting Experiment: description and preliminary results

T. Keenan and R.J. Potts
Bureau of Meteorology Research Centre, Melbourne, Australia
and
J. Wilson
National Center for Atmospheric Research, USA

(Manuscript received December 1990; revised June 1991)

A research program and initial results from a tropical short-term forecasting experiment in Darwin, Australia, are described. The program, involving both real-time forecasting phases combined with ongoing post-analysis phases, is directed at improving our understanding and short-term forecasting capability of tropical weather phenomena. Based on Doppler radar observations, the key forecasts are convective initiation, wind-shift changes and the occurrence of strong winds. Initial results show a systematic relationship between the occurrence of tropical convection and boundary-layer convergence lines visible in the optically-clear air by Doppler radar. This provides the rationale for making probabilistic forecasts of the initiation of convection and wind-shift changes. The results also indicate the utility of Doppler radar in providing timely warnings of the occurrence of strong winds in the zero to three-hour time frame and in identification of microbursts.

Introduction

Significant severe weather events such as thunderstorms, microbursts and tornadoes occur on very short time and space scales, but have a potentially large impact on the population. Detection and forecasting of these short-term meso-β (20–200 km) to meso-γ (2–20 km) scale (Orlanski 1975) events is notoriously difficult and imprecise (e.g. Schlatter 1985; Smith et al. 1986; Szoke and Brady 1987). These events occur below the resolution of most current operational numerical models. Favourable conditions for development can be discerned with numerical models (Mills and Leslie 1986) but precise details in the zero to three-hour period for individual storms are not obtained. Thus the conventional approaches of large-scale numerical weather prediction schemes, often in conjunction with model output statistics (Glahn and Lowry 1972), are generally only applicable for forecast periods beyond three hours (Doswell 1986). For periods of less than three hours, detection of the various phenomena and extrapolation techniques form the basis for most forecasts.

The increasing pressure for accurate short-term prediction of precipitation, dangerous winds, tornadoes and microbursts has prompted several experimental programs. They include the following mid-latitude programs: the Program for Regional Observing and Forecasting Service, as described by Reynolds (1983), undertaken in the United States; the FRONTIERS project described by Browning and Carpenter (1984), conducted in the United Kingdom; and the European PROMIS 600 project of Bodin et al. (1985). Meteorological data from networks of automatic weather stations and remote sensing platforms such as satellite and modern radars have been routed through fast communication and display

Corresponding author address: Dr T. Keenan, Bureau of Meteorology Research Centre, GPO Box 1289K, Melbourne, Victoria 3001, Australia.

systems to provide timely, high-resolution integrated observational data bases suitable for the diagnosis and short-term forecasting problem.

Development of short-term forecasting skills of the type described by Wilson and Roesli (1985), Schlatter et al. (1985), McGinley (1986) and Doswell (1986) is of primary importance. Holland et al. (1987) have implied that the skill of tropical short-term forecasting is low, partly because of the short time and space scales involved with the occurrence of predominantly convective weather. It is postulated that this preponderance of convective weather in tropical locations makes it ideal for the development and testing of the hardware and skills necessary to meet similar short-term forecasting challenges at other locations; i.e., experience gained in short-term forecasting at tropical locations should have ready applicability to analogous convective situations in mid-latitude and subtropical environments. Development of nowcasting skills in the tropics is therefore potentially important from the viewpoint of tropical forecasting *per se* and also for the application of convective-type forecasting skills to mid-latitude convective storms.

Recently, as discussed by Keenan et al. (1988), the National Oceanic and Atmospheric Administration (NOAA)/Tropical Oceans and Global Atmosphere (TOGA) Doppler radar was placed in Darwin as part of the Tropical Rainfall Measuring Mission (TRMM). The use of Doppler radar and associated display technology have important applications for nowcasting, as discussed by Wilson and Carbone (1984), Schlatter (1985), Wilson and Roesli (1985) and Serafin (1987). The availability of this radar provided an ideal opportunity to evaluate its use for mesoscale analysis and forecasting in a tropical environment.

This paper describes preliminary Doppler radar observations and experimental forecasts of convective weather events from the Darwin Area Forecasting Experiment (DAFE) conducted in two phases during March 1989 and March 1990.

Objectives

The scientific objectives of the project were:

(a) To investigate mesoscale forecasting problems in a tropical regime dominated by convective-scale processes. Included as specific areas of research interest were:
  (i) initiation of convective storms in a tropical environment;
  (ii) gust front and sea-breeze evolution and their interaction;
  (iii) characteristics of microbursts and macrobursts;
  (iv) verification and predictability of short-term forecasts.
(b) To evaluate the use of Doppler radar in mesoscale analysis and forecasting for both aviation and severe weather related events.
(c) To investigate forecasting problems and develop forecasting skills using real-time forecasting exercises.
(d) To train forecasters in the use of Doppler radar for short-term forecasting of convective storm events.

The implementation of DAFE was undertaken as a collaborative project by the Bureau of Meteorology Research Centre (BMRC), the National Center for Atmospheric Research (NCAR) and the Bureau of Meteorology's Northern Territory Regional Office (NTRO).

Operations

The experiment was conducted during monsoon break or transition season conditions in Darwin with the first field phase from 1–14 March 1989 and the second from 12–26 March 1990. The purpose of these field phases was to undertake real-time forecasting exercises and to gather data for post-analysis and research.

The airflow over Darwin during these periods was generally dominated at low to mid-heights by easterly winds of continental origin. The surface flow was often westerly, driven by a heat low circulation. The diurnal heating cycle produced a range of sea-breeze, gust front, and topographically-initiated thunderstorms, squall lines and related phenomena, as described by Keenan and Carbone (1989).

Operational analysis and forecasting

Preparation of short-term forecasts on a semi-operational basis was an integral part of the program. These forecasting trials were conducted with the following objectives:

(a) To provide experience with the use of Doppler radar data in the mesoscale analysis and forecasting cycle.
(b) To determine if the results of nowcasting/short-term forecasting research from mid-latitudes could be transferred to an operational environment in the tropics.
(c) To investigate the most useful data types and display systems for tropical nowcasting.
(d) To develop and evaluate conceptual forecast models for the initiation, interaction and motion of thunderstorms.

The forecasting exercises were considered an essential 'test bed' component of the whole project by providing immediate feedback and involvement of forecasters in the development of short-term forecasting procedures. This was considered the optimum way to ensure improvements were obtained in operational diagnosis of current weather and short-term forecasts.

Fig. 1 Location of observational sites and forecast areas (stippled) for DAFE.

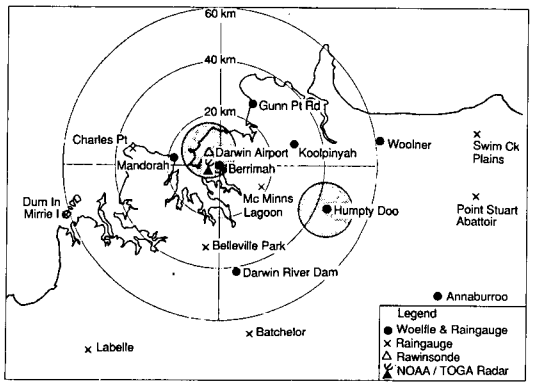

Two circles of 10 km radius around Darwin Airport and Humpty Doo were selected as the primary forecast areas. As shown in Fig. 1, these two areas were close enough to the NOAA/TOGA radar for reliable monitoring of the planetary boundary layer (PBL) structure and far enough apart to provide independent forecasts.

The following forecast products were prepared for each area:

(a) Probability of occurrence of storm activity within the area based on: (i) convective storm initiation associated with convergence lines; and (ii) advection of storms into the forecast areas.
(b) Alerts of microburst development*.
(c) Significant wind shifts (a direction shift of 30° or more with wind speed greater than 7 m s^{-1} before or after the change) or wind gusts greater than 20 m s^{-1}.

A storm was defined as a cell with an effective reflectivity factor exceeding 40 dBZ_e†. The forecasts were issued hourly from 1300 LST to at least 2000 LST and were valid for three-hour periods. Forecasts for storm occurrence in the two areas were in the form of subjective probability statements based on storm advection and possible initiation of convection. All forecast probabilities were referenced by the forecasters to the climatological probability of occurrence of rainfall at the particular time of day, as given by Fraedrich and Leslie (1988) for Darwin. That is, after consideration of all available information, the climatological probability of rainfall provided a consistent basis on which the different forecasters had to grade their assessment for storm occurrence.

*Following Wilson et al. (1984), a microburst is defined as a divergent outflow with a differential velocity of 10 m s^{-1} or greater over a radial distance of 4 km or less. Larger scale outflow events are defined as macrobursts.

†This corresponds to a rainfall rate (R) of approximately 12 mm h^{-1} based on the relationship $Z_e = 200\ R^{1.6}$ following Marshall and Palmer (1948).

Storm occurrence forecasts were valid for three-hour intervals. Following Mueller and Wilson (1989), the three-hour forecast period was further split to provide:

(a) Probabilities of events within each 15-minute interval for the first hour.
(b) Probabilities of event occurrence within the two 30-minute intervals for the second hour.
(c) An outlook probability for the last hour.

Alerts were prepared for microbursts when they could be detected. The location, difference in radial velocity, and shear associated with these systems were recorded. No attempts at forecasting microburst occurrence were made.

Lead times for significant wind-shift forecasts were variable and depended on the information available to the forecaster. Forecasts of the expected wind speed and direction were prepared.

Forecasts were originated from the Darwin Regional Forecast Centre (RFC). No forecasts were made public. Both researchers and local forecasters were involved in producing the short-term forecasts. A number of worksheets was completed during each shift to provide a record of the forecast process and the logic behind each forecast.

The forecasts derived in the operational trial enabled some comparison with the following Bureau of Meteorology products:

(a) The severe thunderstorm advice—a public forecast valid over three hours issued when gusts in excess of 20 m s^{-1} are expected in the Darwin city area.
(b) Aviation forecasts and warnings—the Terminal Aerodrome Forecast (TAF) valid for 24 hours, the Trend-Type Forecast (TTF) valid for three hours, and the Airport Warning, all provided for Darwin Airport. The latter is issued when winds in excess of 20 m s^{-1} are expected at the airport.

Observing facilities

The observing network for the 1989 experiment is shown in Fig. 1. The basic observational tool was the NOAA/TOGA 1.65° beamwidth, 5.3 cm wavelength (C-band) radar located at Berrimah. In support of the real-time forecasting component, a forecasting team was located in the RFC where ancillary meteorological information was available. One member of the team was located at the Doppler radar to optimise radar scans and interpret the high resolution radar data display. A lower resolution Bureau of Meteorology microcomputer-based radar data system (PC-RAPIC) was used to display the Doppler radar data in the RFC. The PC-RAPIC system at the RFC displayed reflectivity and Doppler velocity scans for a single level and had a looping capability. Since the PC-RAPIC system could not display multiple plan position indicator (PPI) scans or range height indicator (RHI) scans, volumetric PPI scans and RHI scans were undertaken continuously at the

NOAA/TOGA radar and the relevant features were communicated verbally to the RFC.

As discussed by Wilson and Schreiber (1986), and as will be shown here, radar-detected 'clear air' echoes in the PBL can highlight many flow features useful in short-term forecasting of convective initiation. Thus, when using Doppler radar it is essential that the radar have sufficient sensitivity to enable the detection of clear air echoes in the PBL. These non-precipitation echoes result from refractive index fluctuations, clouds and insects. For a C-band radar, the analysis of Pratte and Keeler (1986) indicates that echoes from insects range from about -7 dBZ_e to 19 dBZ_e; for clouds, reference reflectivities vary from -19 dBZ_e for stratus, -14 dBZ_e for trade wind cumulus to approximately 11 dBZ_e for cumulus congestus. The Bragg scatter from refractive index fluctuations is approximately -35 dBZ_e. Thus, for the NOAA/TOGA radar, echoes between -14 and 19 dBZ_e for ranges between 10 and 50 km are interpreted as clear air signatures of insects.

Table 1. Operating parameters for NOAA/TOGA Doppler radar.

Wavelength	5.33 cm
Beamwidth	1.65°
Transmitter power	250 kW
Pulse width	0.5 and 2.0μ s
PRF	400 and 1100 hz
Nyquist frequency	5.33 and 14.74 m s^{-1}

Table 1 shows the operating parameters that were used for the NOAA/TOGA radar. The pulse repetition frequency (PRF) was limited to 400 Hz for scans using the 2.0 μs transmitter pulse, owing to radar transmitter duty cycle restrictions. When using the 0.5 μs transmitter pulse, the PRF was set to 1100 Hz. These PRFs result in Nyquist* velocities of 5.3 and 14.7 m s^{-1} respectively. The scanning program for the radar was designed to enable optimum clear air detection at low elevations, the detection of initial cell development at mid-levels, and the ability to examine the reflectivity and velocity structure of thunderstorms and squall lines. The program comprised 360° volumetric PPI scans at 9 tilts using 'short pulse/high PRF' conducted at five-minute intervals, followed by a 360° PPI scan at 0.8° elevation using 'long pulse/low PRF'. RHI scans were conducted as considered necessary.

*The maximum unambiguous frequency that can be measured with a Doppler radar is limited to half the PRF so the maximum unambiguous Doppler velocity , which defines the Nyquist interval, is given by

$$V_{max} = \pm \frac{(PRF)\lambda}{4}$$

where λ is the radar wavelength.

The 'long pulse/low PRF' scan provided greater sensitivity for the detection of clear air echoes because more power is transmitted. Also, because of the lower Nyquist interval, there was an improved velocity resolution when the wind speeds were weak, enabling convergent boundaries associated with the developing sea-breeze to be detected more easily. Although less sensitive, the 'short pulse/high PRF' scan made the analysis of velocity fields much easier when wind speeds increased, with squall lines for example, as significant velocity aliasing was evident on the low PRF scan.

Three-hourly, and occasionally hourly, Japanese Geostationary Meteorological Satellite (GMS) data were available at the RFC. These data were useful for defining initial development of cumulus convection before it was detectable by radar, the variability in low-level moisture and upper-level cloud cover. An Australian Region McIDAS station (LeMarshall et al. 1987) was used to display satellite data and synoptic-scale analysis and prognostic data.

Upper air rawinsondes were undertaken from Darwin Airport at 0730 LST, 1330 LST and 1930 LST for the duration of the experiment. A wind-only sounding was made at 0130 LST.

Real-time surface data were available continuously from Darwin Airport, and every three hours from the NTRO meso-synoptic network. A mesoscale, eight-station Woelfle anemograph network (2 m above ground level) was established, as shown in Fig. 1, for post-analysis and verification studies. This network formed an outer circle on the two basic forecast areas and provided *in situ* wind measurements for the verification studies. Woelfle anemographs record wind-run rather than wind speed and so significantly underestimate the strength of short-duration strong winds. Nevertheless, the anemograph data provide a good indication of the time of wind shifts. The TRMM raingauge network data (Keenan et al. 1988) were available for post-analysis and other related studies.

Examples of nowcasting events in Darwin

Nowcasting in Darwin during DAFE will be described in this section with a brief analysis of the weather events that were observed on 5 March 1989. The objective here is to provide examples of the observational data base available to the experiment, the applicability of the observational tools to nowcasting and some of the problems associated with nowcasting tropical convective-scale weather.

The synoptic situation over Australia on 5 March 1990, as shown in Fig. 2(a), was typical for the transition season. At the surface, the subtropical ridge lay south of the continent with a high

Fig. 2 (a) Streamline analysis for 850 hPa at 2300 UTC 4 March 1989. (b) The 1330 LST rawinsonde sounding from Darwin Airport. Each full barb represents 5 m s^{-1}, each half barb 2.5 m s^{-1}.

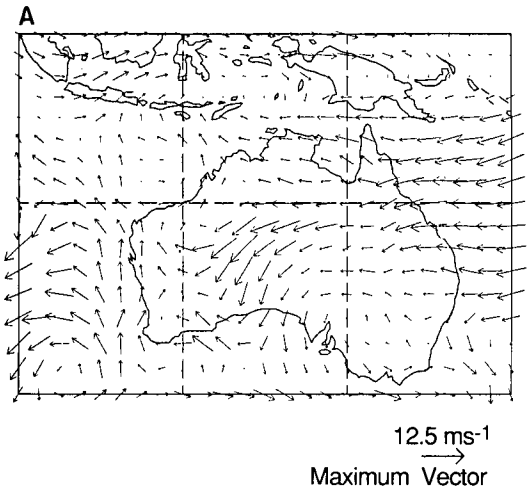

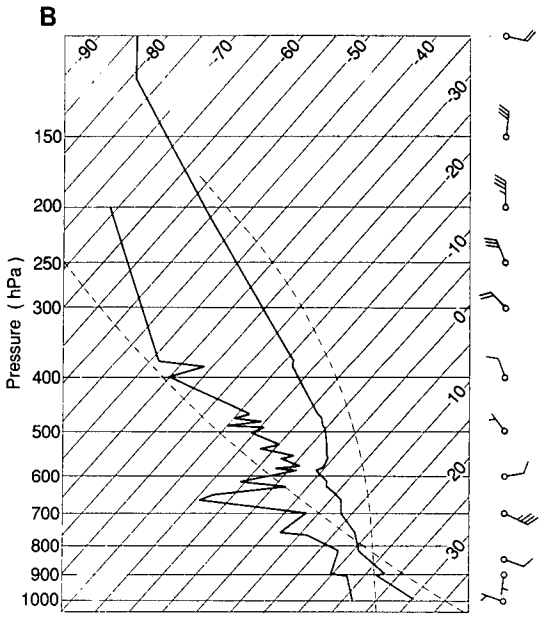

pressure ridge extending up the east coast. A shallow heat trough extended from a low over the northwest of Western Australia to just west of Darwin. The monsoon trough was north of Darwin near latitude 9°S. As shown in Fig. 2(b), there was an easterly flow in the low to middle levels over Darwin with a 17.5 m s^{-1} maximum near 700 hPa that extended across northern Australia. The upper troposphere contained north to northwesterly flow. The 1330 LST temperature sounding in Fig. 2(b) showed stable layers at 900 hPa and 600 hPa and dry layers near 650 hPa and above 450 hPa. The most significant change in the sounding throughout the day was an increase between 0730 LST and 1330 LST of 2.5 g kg^{-1} in the average moisture content for the surface to 700 hPa layer and a breakdown in the low-level stability. The Convective Available Potential Energy (CAPE), as defined by Moncrieff and Green (1972), and Convective Inhibition (CIN), as defined by Colby (1983), ranged respectively from 0 (−335) J Kg^{-1} at 0730 LST to 970 (−27) J kg^{-1} at 1330 LST and were in the low to moderate range for Darwin (Keenan and Carbone 1989).

Evolution of PBL clear air echoes

The Doppler velocity display, in conjunction with the reflectivity display, enables identification and analysis of PBL flow fields including the location of significant wind shift and convergence zones. In this case, it was possible to monitor the evolution and interaction of the sea-breeze front and numerous thunderstorm-initiated gust fronts. The evolution of the main boundaries on 5 March is illustrated in Fig. 3 and selected Doppler radar displays are shown in Fig. 4. For this analysis, a

Fig. 3 Isochrones showing the evolution of radar-detected clear air convergent boundaries during the afternoon and evening of 5 March 1989. Evolution is shown for (a) 1337–1715 LST, (b) 1726–1847 LST and (c) 1922–2055 LST.

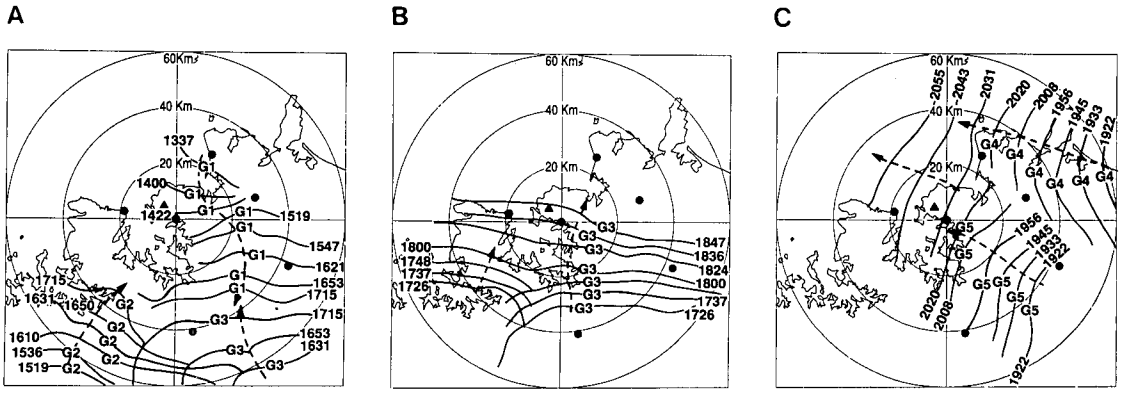

Fig. 4 Selected reflectivity (left-hand side) and radial velocity fields (right-hand side) at 0.8° elevation from NOAA/TOGA Doppler radar for 5 March 1989 at (a) 1337 LST, (b) 1631 LST, (c) 1715 LST, (d) 1748 LST, (e) 1932 LST and (f) RHI scan along 120° azimuth at 2008 LST. Reflectivity (dBZ_e) and radial velocity ($m\ s^{-1}$) scales are indicated below each frame. Range rings are at 20 km intervals and RHI vertical axis is to 20 km height. For the Doppler velocity fields, warm colours indicate radial motion away from the radar and cool colours radial motion toward the radar. The location of the major clear air boundaries (G1-G5) and the microburst (MB) are indicated.

(a)

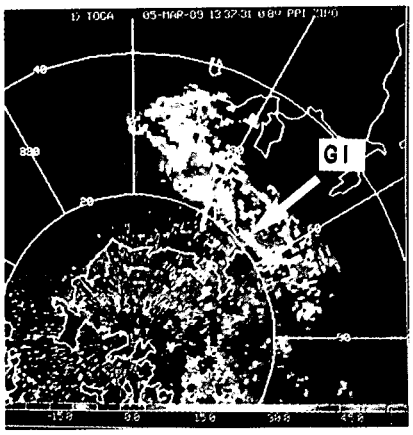

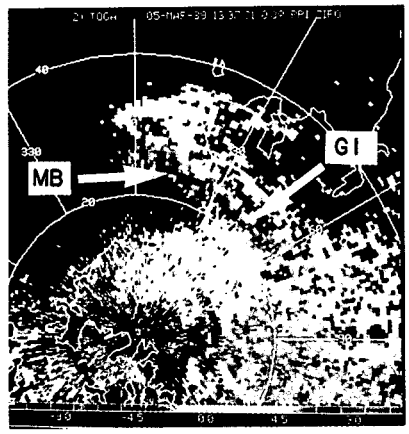

(b)

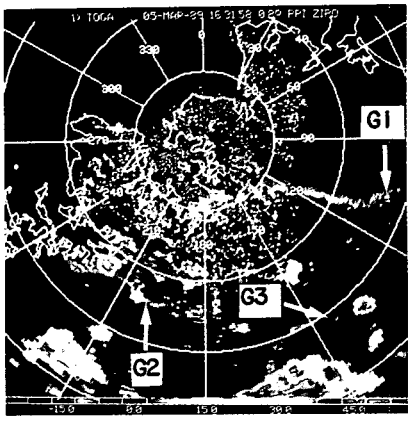

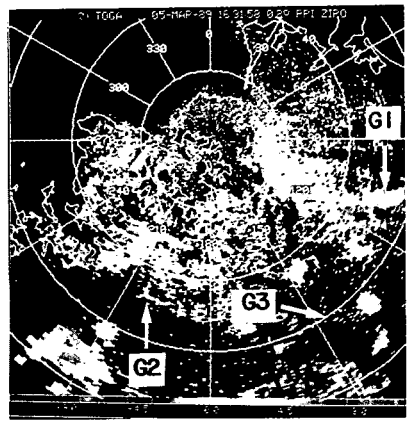

(c)

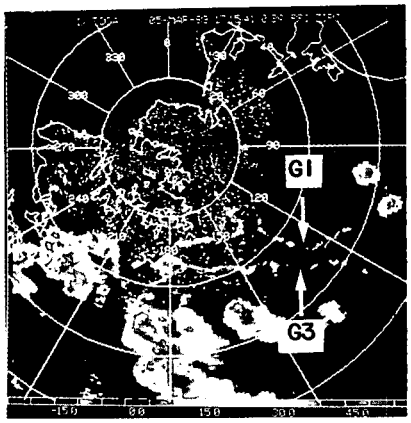

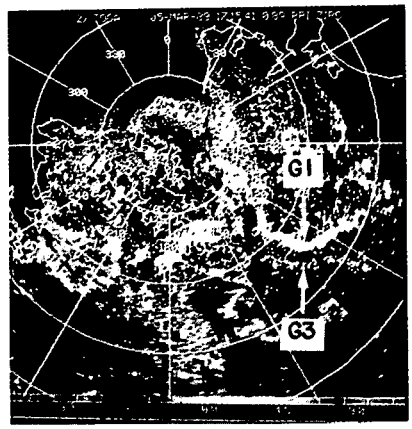

Fig. 4 Continued.

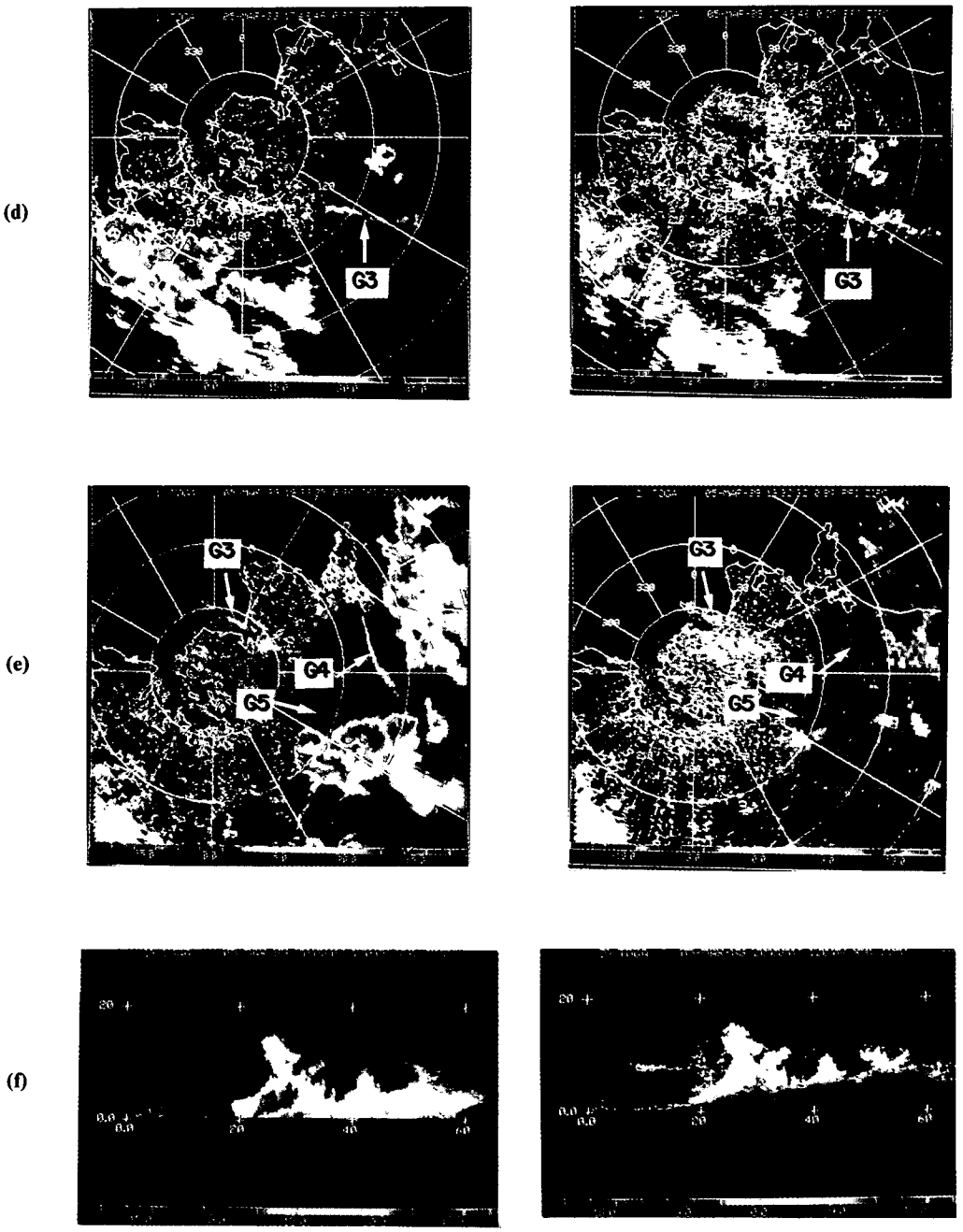

boundary was defined as a moving thin line of reflectivity greater than -14 dBZ$_e$ and less than 24 dBZ$_e$, exhibiting the characteristic appearance of a sea-breeze convergence zone or gust front as described by Wilson and Carbone (1984), Simpson (1987) and Mahoney (1988), and having a length at least an order of magnitude greater than its width (the latter was typically less than 4 km).

Figure 3 shows that the evolution of the clear air boundary signatures was complex. Initial activity (G1) was associated with the thunderstorm development 30 km to the northeast at 1325 LST, as evident in Fig. 4(a). This source thunderstorm was thought to be initiated by sea-breeze convergence in the region of Gunn Point, which was not evident on radar owing to a lack of clear air returns. At 1337 LST, G1 (Fig. 4(a)) extends to the

southeast of the thunderstorm cell and is associated with confluence in the radial velocity field. The 'fine line' is interpreted as the clear air signature of a convergence zone. This convergence zone moved to the south at a mean speed of approximately 4.0 m s^{-1}. It appears to have been reinforced by outflows from thunderstorms east of Gunn Point, together with the sea-breeze based on the interpretation of the Doppler radar data and the wind information provided by the anemograph network.

Such sea-breeze echoes were often observed at Darwin during the afternoon with the inland penetration of the sea-breeze. RHI data taken through similar southward-moving echoes (not shown) indicate weak echoes to approximately 1 km deep, an elevated head structure with overhanging nose at the leading edge and a trailing turbulent wake region. The structure is characteristic of both thunderstorm outflows and sea-breeze generated density currents, as described by Simpson (1987) and Mahoney (1988). The internal boundary layer associated with the sea-breeze is evident in the 1330 LST temperature sounding as a well-mixed layer capped by an inversion at 1 km (Fig. 2).

The passage of G1 to the south is evident on the anemograph traces as a shift in the surface airflow to a northerly direction (Fig. 5). Variations with location are apparent; e.g., at Darwin Airport, the wind shift was more gradual owing to the gradual development of the sea-breeze circulation. However, the inland movement of G1 and associated wind shifts were consistent with the passage of a gust front which is reinforced by the typical northwest sea-breeze which occurs in Darwin.

During the afternoon a line of thunderstorms developed well south of the radar and generated gust fronts, G2 and G3, which merged and moved to the north at speeds between 2–8 m s^{-1}. These gust fronts are indicated in Figs 4(b) to (e) starting 60 km to the south-southwest of the radar. The mechanism responsible for the initial development of these thunderstorms is not known. By 1715 LST (Fig. 4(c)), an active line of thunderstorms had developed 40–60 km south of the radar and this was closely related to the passage of G2/G3. Outflow from cells within this line of storms appears to have reinforced the flow associated with the gust fronts.

At 1726 LST, the southward-moving conver-

Fig. 5 Anemograph traces for 5 March 1989 from (a) Gunn Point, (b) Darwin Airport, (c) Berrimah and (d) Humpty Doo. In Woelfle anemograph traces (a, c, d) the wind direction is given in the lower frame and the wind-run in the upper frame. The wind speed is given by the gradient of the wind-run record. Times are LST.

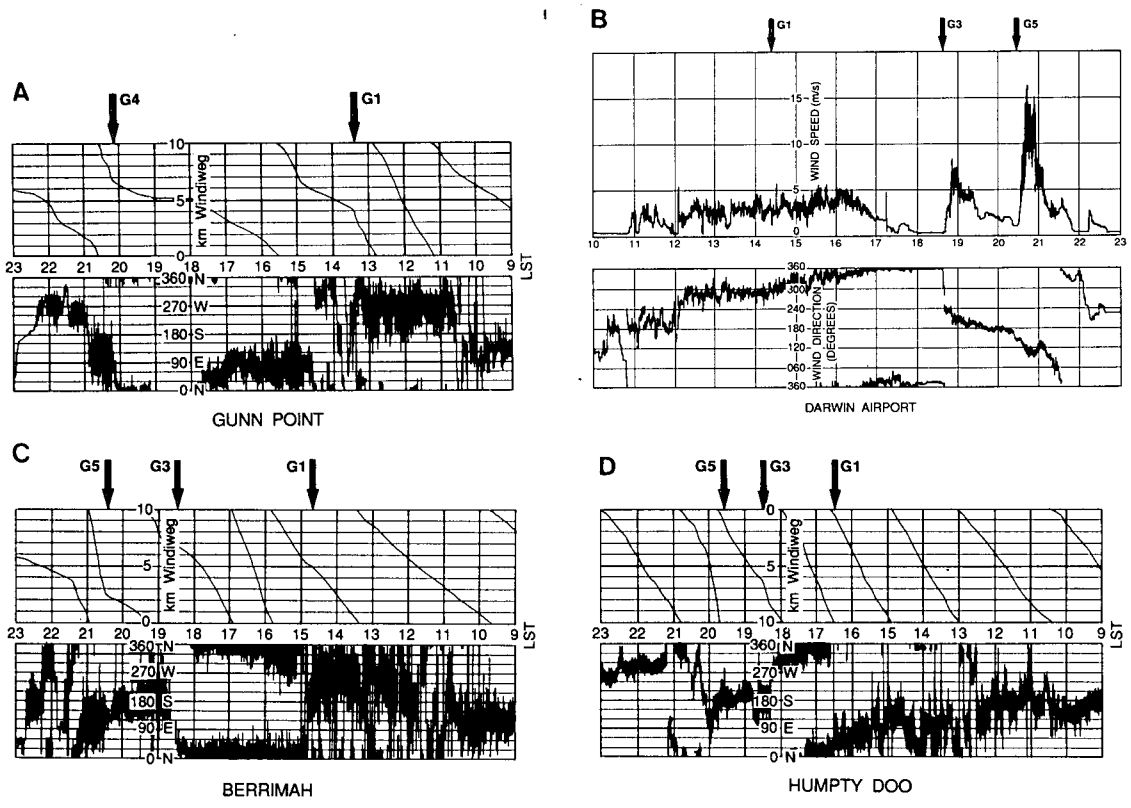

gence line G1 and the northward-moving gust front G2/G3 collided 31 km south of the radar. As shown in Fig. 4(d), G2/G3 continued to move north at 6–7 m s^{-1} and was still evident until 2031 LST when it was approximately 15 km north of the radar (Fig. 4(e)). G1 was not discernible after the collision with G2/G3. No further storm development occurred in the vicinity of G3 as it moved north over the radar. This was consistent with the presence of a more stable atmosphere following the southward movement of G1 earlier in the day.

The northward passage of G3 is evident in the anemograph traces (Fig. 5) with the southerly change moving over Humpty Doo at 1820 LST, and Berrimah and Darwin Airport at around 1840 LST.

The next major gust front activity was observed between 1910 and 2100 LST (Fig. 3(c)). A line of thunderstorms developed well east of the radar and these moved westward over Darwin at 11–12 m s^{-1}. By 1933 LST (Fig. 4(e)), gust fronts G4 and G5 were evident on the radar 5–10 km ahead of the associated storms. These gust fronts merged at 2030 LST approximately 25 km northeast of the radar and moved over Darwin ahead of a major squall line. The maximum wind speed recorded at Darwin Airport with the passage of the squall line was 16.5 m s^{-1} (Fig. 5(b)).

Other convergent boundaries were evident on the Cox Peninsula south of Cnarles Point from 1337 LST to 1422 LST (not shown). These boundaries were thought to be the result of sea-breeze convergence.

As the preceding discussion has indicated, the motion and origin of these clear air signatures and associated weather during the afternoon of 5 March were variable and complex. A more detailed examination of the relationship of these echoes to convective initiation and wind-shift changes follows.

Convective initiation

The relationship of convective initiation to convergence boundaries has been studied extensively by Wakimoto (1982), Wilson and Carbone (1984) and Mueller and Carbone (1987). Wilson and Schreiber (1986) found that 79 per cent of storms were initiated in close proximity to radar-observed PBL convergence lines over a 5000 km^2 area east of the Colorado Rocky Mountains. Colliding covergence lines initiated new storms or intensified existing storms in 71 per cent of cases. These studies are important because they document a relationship between the development of convection and features that can be monitored. In addition, simple advection of these convergence boundaries evident in the clear air enables forecasts of the probable location of convective initiation. Given the lifetime of these signatures, it is possible for the first time to undertake forecasts of convective initation with lead times up to three hours.

The description of the clear air signatures undertaken in the previous section shows a relationship with the initiation of convection in the vicinity of Darwin. At 1631 LST, G1 is evident clearly as a 'fine line' which extends from a point 19 km south of the radar to the east. As G1 moved south, new convective cells developed 8 km northwest of Darwin at 1422 LST, 25 km northeast of the radar at 1547 LST and 60 km to the east at 1715 LST (Fig. 4(c)). The development of these cells was related closely to the passage of the convergence zone.

As evident from Fig. 4, the most significant outbreak of convective activity had occurred by 1715 LST, 40–60 km south and southwest of Darwin. Inspection of the radar data and Fig. 3 shows that this major outbreak of convection was closely linked to the passage of gust front G2/G3. In some cases the formation of convective cells occurred directly on gust fronts; for example the storms which developed at 1631 LST on G2 45 km southwest of the radar and on G3 64 km southeast of the radar. In other cases, cell formation was evident some 10–30 minutes after the passage of the gust fronts, consistent with the findings of Wilson and Schreiber (1986). The storms visible at 1715 LST between 40 and 60 km south of the radar developed shortly after the passage of G3. Irrespective of exact timing, the important point is that the most significant area of convective initiation was associated with the occurrence of gust front activity.

In this example, the collision between G1 and G2/G3 failed to produce any significant convection to the southeast of the radar. The reason for this is not obvious and most likely impossible to discern from the data available to this study.

For the two forecast areas employed in the study, the southward-moving convergence line G1 failed to produce major convective activity. Forecasts issued for the Humpty Doo area between 1500 and 1600 LST contained an increased probability of convective initiation between 1600 LST and 1730 LST associated with the passage of G1. Similarly, the collision of G1 and G2/G3 at 1726 LST and the subsequent northward movement of G2/G3 were primary reasons for increasing the probability of convective initiation near Humpty Doo between 1700 LST and 1830 LST. No convective initiation was observed in the forecast area from these sources although convective cells developed east of the Humpty Doo area. These cells weakened before advecting into the area (Fig. 4(d)).

These failures reflect the difficulties in short-term forecasting of storm initiation and movement and the need for studies into the details of storm initiation by boundary-layer convergence lines.

Wind-shift changes

When the clear air returns are discernible, sharp wind-shifts associated with gust fronts, thunderstorms, squall lines and sea-breeze circulations can be monitored readily on the Doppler display.

Examination of the radar data (Fig. 4) and the surface winds observed at Berrimah (Fig. 5) on 5 March provides an example of the utility of the Doppler data in the diagnosis of the mesoscale wind flow. As discussed earlier, a weak westerly sea-breeze was established by 1230 LST. This is evident also in the Doppler velocity field at 1337 LST (Fig. 4(a)), which indicates radial inflow to the north and northwest at short range. Farther inland, to the southeast, radial inflow is evident, suggesting a southeasterly component to the surface flow. This suggests that the sea-breeze has penetrated inland a short distance with the boundary between the two flows located close to the radar.

The ability to observe the mesoscale airflow in clear air and monitor the movement of fine lines associated with wind shifts (Fig. 3) enables a clear interpretation and possible forecasts of mesoscale wind shifts. For example, the initial 1440 LST change at Berrimah is due to the southward passage of G1. The 1840 LST change was due to the northward passage of G3 and the change at 2030 LST was associated with the passage of G5. Forecasts of the time of wind-shift changes at 1840 LST and 2030 LST are readily available by simple extrapolation of the fine line positions summarised in Fig. 3. For example, the velocity of G3 at 1715 LST (i.e. prior to the collision with G1) by simple extrapolation gives an estimated time of arrival at Berrimah of 1837 LST. At 1748 LST, based on the movement after the collision, the estimated time of arrival of G3 at Berrimah was 1840 LST. The actual time of arrival was approximately 1840 LST. Extrapolation of G5 at 1945 LST gives a time of arrival at Berrimah of 2040 LST. This compares with the actual time of arrival of 2030 LST indicating the squall line accelerated. Such acceleration can be monitored continuously with the radar.

Doppler data can be used to assess the severity of winds associated with the passage of squall lines. Doppler estimates of the wind behind G3 were southerlies in the range 6–8 m s^{-1}. At Darwin Airport, the Dines anemograph (Fig. 5(b)) shows a maximum wind gust of 8.5 m s^{-1} associated with a southerly change at 1840 LST, which is in good agreement with the Doppler radar observation. Figure 4(e) indicates east to southeast winds in the range 15–20 m s^{-1} associated with the passage of G5. At Darwin Airport, the Dines anemograph recorded a maximum wind speed of 16.5 m s^{-1} with the squall line, also in good agreement with the Doppler radar observations.

Vertical structure

Another important mode of Doppler radar use is evident from the RHI data at 2008 LST shown in Fig. 4(f), taken perpendicular to the approaching squall line. In this case, the combination of the reflectivity structure and the associated Doppler-measured radial flow fields enable the forecaster to diagnose several important properties of the approaching storm:

- The origin of air associated with wind shifts and the strength and timing of the wind-shift changes.

In this case, a rear-to-front circulation is evident, transporting 3 km origin air to the PBL at the leading edge of the storm. Approaching velocities in the range of 15–20 m s^{-1} are evident. Diagnosing this process enables the sounding data to be used to make a first-order estimate of the maximum wind speeds associated with the squall passage. From Fig. 2 (b), the 700 hPa flow was 17.5 m s^{-1}. Downward exchange of this momentum would imply surface wind speeds of at least 17.5 m s^{-1} with the passage of the storm. This estimate agrees well with the maximum gust observed at Darwin Airport.

In addition, the rear-to-front flow is seen to extend into the cold pool and reach some 10 km ahead of the leading convective cells. This gives an indication of the time at which the wind shift will occur in relation to the onset of the precipitation.

- The internal draught structure of the system can be viewed and inferences made on the likelihood of system maintenance or dissipation.

In Fig. 4(f), strong front-to-rear flow is seen overlaying the descending rear-to-front flow. Successive generations of the convective cells can be seen at 25 km, 42 km and 52 km. In this case, the most recent cell has a strong updraft (inferred from the front-to-rear flow) which extends to 17–18 km. The motion fields, in combination with the reflectivity cores, indicate a strong system. In addition, the generation of new cells over the forward-propagating density current can be inferred. All these factors are crucial in assessing the likely life cycle of the storm.

In summary, these examples have shown how the forecaster can readily obtain accurate forecasts of wind shifts and wind strengths associated with movement of gust fronts and squall lines with a 1–2 hour lead time. With regard to the squall line, it was possible to determine that non-severe wind gusts (<20 m s^{-1}) were associated with these storms. The ability to discriminate severe and non-severe thunderstorm activity is an important aid to the forecaster which cannot be inferred from conventional radar data alone.

Horizontal wind shear and microbursts

The detection of low-level horizontal wind shear conditions hazardous to the operation of aircraft represents an extremely important nowcasting application. The occurrence of such low-level shear has been responsible for a number of aircraft accidents (Fujita 1985). Following Fujita (1981), typical spatial scales for these microburst (macroburst) events range from 1 to 4 km (4 to 10 km) and the temporal scale is typically 2 to 20 minutes (10 to 60 minutes). Many examples of such microburst/macroburst events were observed during the nowcasting project.

A study of microburst characteristics undertaken by Potts (1991) using the Doppler radar data suggests that an average of 5–6 microbursts per day occurs within 40 km of Darwin during convectively active 'break' periods. The existence of a microburst problem at Darwin, and for that matter in tropical locations, was not well documented until the Doppler observational program commenced. Nowcasting, based on standard weather watch radars and meso-networks of anemometers, cannot readily discern the existence of these phenomena.

The following example demonstrates the importance of Doppler radar observations for detection of microburst phenomena. At 1337 LST (Fig. 4(a)), a sea-breeze initiated thunderstorm is evident 25 km to the north-northeast of Darwin. Inspection of the Doppler data shows this storm is producing a microburst. The advancing and receding velocities indicate a difference of 19.5 m s^{-1} over 4 km or a radial shear of 5×10^{-3} s^{-1}. The intensity of this horizontal shear is similar to the average of 5.2×10^{-3} s^{-1} observed for Colorado microbursts in the Wilson et al. (1984) study of Joint Airport Weather Studies data. The Woelfle anemograph sited at Gunn Point (Fig. 5(a)) shows a shift in the wind at 1310 LST from a westerly to a northerly. The wind speed is estimated at 5 m s^{-1}, although the peak wind speed may have been considerably greater. The winds then shifted southerly by 1330 LST, weakened and became quite variable until 1430 LST. At 1400 LST (not shown), the divergent outflow was still evident on radar, with a radial velocity differential of 10 m s^{-1} over 4 km or a radial shear of 2.5×10^{-3} s^{-1}.

Summary and future development

This paper has presented a preliminary analysis of events observed from the first Doppler radar-based mesoscale forcasting and nowcasting study in the tropics. The preliminary results presented herein have shown that Doppler radar can make a valuable contribution to short-term forecasting in tropical locations. The authors have shown that clear air radar signatures can be used to monitor gust front evolution and related directly to the location of thunderstorm generation and the occurrence of wind-shift changes. Examination of basic Doppler data has been shown to give a clear indication of the strength of winds associated with thunderstorms, microbursts and squall lines.

Current research is directed at studies related to the characteristics of gust front evolution and its relationship to storm development. Diagnostic verification studies are also underway to evaluate the skill of the real-time forecasts.

Major challenges remain in this field. Future work will be directed at improving the data base, the real-time display capability, and more objective analysis and diagnostic capabilities using an integrated workstation concept. Experience suggests that satellite, radar, mesonet and rawinsonde data are required in a user-friendly display system that enables the forecaster to undertake detailed analyses and simple extrapolation-type forecasts. Extending forecasts past the 0–3 hour time period, where extrapolation and detection are the key forecast methodologies, depends on the scale and type of phenomenon (Doswell 1986; Browning 1989) but ultimately numerical prediction approaches should be evaluated as part of the forecast process. Development of numerical prediction approaches that can be used interactively for such mesoscale forecasts in real-time is an area requiring considerable research.

Another problem encountered during DAFE was the lack of clear air echo signatures during a period of westerly monsoon flow of oceanic origin, i.e. during monsoonal reversal from the continental origin transition season flow discussed herein. Under such circumstances, the availability of real-time mesonet and satellite data is crucial in defining local circulations and the potential for convective initiation.

Acknowledgments

This work was supported by Mike Manton (BMRC), Rit Carbone (NCAR) and Jim Arthur (NTRO). The development work undertaken by Phil Purdam and Ken Glasson to provide the remote display of the Doppler radar data on PC-RAPIC is gratefully acknowledged.

References

Alberty, R., Holitza, F.J., Ackley, M.H., Smart, J.R., Lipschutz, R.C., Roberts, W.F. and Leep, K.J. 1983. PROFS Doppler radar data processing system, Part I: Design and implementation with application to NEXRAD algorithms. *NOAA Tech. Memo. ERL ESG-3*, Environmental Science Group, Boulder CO, 143pp.

Bodin, S., Gollvik, S., Gustafsson, N. and Törnevik, T. 1985. Development of analysis and forecasting methods for PROMIS 600. *ESA Journal, 9*, 227–33.

Browning, K.A. 1989. The mesoscale database and its use in mesoscale forecasting. *Q. Jl R. met. Soc., 115*, 717–62.

Browning, K.A. and Carpenter, K.M. 1984. FRONTIERS five years on. *Met. Mag., Lond. 113*, 282–7.

Colby, F.P. Jr 1983. Convective inhibition as a predictor of the outbreak in convection in AVE-SESAME II. Preprints, *13th Conf. on Severe Local Storms*, Tulsa, Amer. Met. Soc., 324–7.

Doswell, C.A. III. 1986. Short-range forecasting. *Mesoscale Meteorology and Forecasting*, P.S. Ray (ed.), Amer. Met. Soc., 678–719.

Falls, R. 1990. Perspectives on operational weather forecasting and warning in tropical Australia. *Aust. Met. Mag., 38*, 53–63.

Fraedrich, K. and Leslie, L.M. 1988. Real-time short-term forecasting of precipitation at an Australian tropical station. *Weath. forecasting, 3*, 104–14.

Fujita, T.T. 1981. Tornadoes and downbursts in the context of generalized planetary scales. *J. Atmos. Sci., 38*, 1511–34.

Fujita, T.T. 1985. *The downburst, microburst and macroburst.* University of Chicago, Illinois, 60637, NTIS PB-148880, 122pp.

Glahn, H.R. and Lowry, D.A. 1972. The use of model output statistics in objective weather forecasting. *Jnl appl. Met., 11*, 1203–11.

Holland, G.J., Leslie, L.M., Fraedrich, K. and Love, G.B. 1987. The challenge of very short range forecasting in the tropics. *Proc. Symp. Mesoscale Analysis and Forecasting*, Vancouver, Canada, 17–19 August, 1987, ESA SP-282, 287–95.

Keenan, T.D., Holland, G.J., Manton, M.J. and Simpson, J. 1988. TRMM ground truth in a monsoon environment: Darwin, Australia. *Aust. Met. Mag., 36*, 81–90.

Keenan, T.D. and Carbone, R.E. 1989. A preliminary morphology of convective systems in tropical northern Australia. *24th AMS Conference on Radar Meteorology*, Tallahassee, Fl, 640–4.

Le Marshall, J.F., Stirling, L.J., Davidson, R.F. and Hasset, M.J. 1987. The Australian region McIDAS. *Aust. Met. Mag., 35*, 55–64.

Mahoney, W.P. 1988. Gust front characteristics and the kinematics associated with interacting thunderstorm outflows. *Mon. Weath. Rev., 116*, 1474–91.

Marshall, J.S. and Palmer, W.M. 1948. The distribution of raindrops with size. *J. Met., 5*, 165–6.

McGinley, J. 1986. Nowcasting mesoscale phenomena, *Mesoscale Meteorology and Forecasting*, P.S. Ray (ed.), Amer. Met. Soc., 657–88.

Mills, G.A. and Leslie, L.M. 1986. A mesoscale NWP study of a convective outbreak over South Australia. *Short and Medium Range Numerical Weather Prediction, Collection of Papers Presented at the WMO/IUGG Symposium*, Tokyo, 4–8 August.

Moncrieff, M.W. and Green, J.S.A. 1972. The propagation and transfer properties of steady convective overturning in shear. *Q. Jl R. met. Soc., 98*, 336–52.

Mueller, C.K. and Carbone, R.E. 1987. Dynamics of a thunderstorm outflow. *J. Atmos. Sci., 44*, 1879–98.

Mueller, C.K. and Wilson, J.W. 1989. Evaluation of the TDWR nowcasting experiment, *24th AMS Conference on Radar Meteorology*, Tallahassee, Fl, 224–7.

Orlanski, I. 1975. A rational subdivision of scales of atmospheric processes. *Bull. Am. met. Soc., 56*, 527–30.

Potts, R. 1991. Microburst observations in tropical Australia. *4th International Conference on Aviation Weather Systems*, Paris, France, J67–72.

Pratte, J.F. and Keeler, R.J. 1986. Sensitivities of operational weather radars. *23rd AMS Conference on Radar Meteorology and Cloud Physics*, September 22–26, Snowmass, Colorado, JP333–336.

Reynolds, D.W. 1983. Prototype work station for mesoscale forecasting, *Bull. Am. met. Soc., 64*, 264–73.

Schlatter, J.W. 1985. A day in the life of a modern mesoscale forecaster, *ESA Journal, 9*, 235–56.

Schlatter, J.W., Schultz, P. and Brown, J.M. 1985. Forecasting convection with the PROFS system: Comments on the summer 1983 experiment. *Bull. Am. met. Soc., 66*, 802–809.

Serafin, R.J. 1987. New nowcasting opportunities using modern meteorological radar. *Proc. Symp. Mesoscale Analysis and Forecasting*, Vancouver, Canada, 17–19 August 1987, ESA SP-282.

Simpson, J.E. 1987. *Gravity Currents: In the Environment and the Laboratory*, Ellis Horwood Limited, 244pp.

Smith, D.L., Zuckerberg, F.L., Schaefer, J.T. and Rasch, G.E. 1986. Forecast problems: The meteorological and operational factors. *Mesoscale Meteorology and Forecasting*, P.S. Ray (ed.), Amer. Met. Soc., 793pp.

Szoke, E.J. and Brady, R.H. 1987. The use of advanced data sets in short-range forecasting of the development of a tornadic thunderstorm along a mesoscale convergence zone. *Proc. of International Symposium on Mesoscale Analysis and Forecasting*, Vancouver, Canada, 17–19 August, 67–72.

Wakimoto, R.M. 1982. The life cycle of thunderstorm gust fronts as viewed with Doppler radar and rawinsonde data. *Mon. Weath. Rev., 110*, 1060–82.

Wilson, J.W. and Carbone, R. 1984. Nowcasting with Doppler radar: The forecaster-computer relationship. *Proc. Nowcasting-II Symposium*, Norrkoping, Sweden, 3–7 September (ESA SP-208).

Wilson, J.W., Roberts, R.D., Kessinger, C. and McCarthy, J. 1984. Microburst wind structure and evaluation of Doppler radar for airport wind shear detection. *Jnl Clim. appl. Met., 23*, 898–915.

Wilson, J.W. and Roesli, H.P. 1985. Use of Doppler radar and radar networks in mesoscale analysis and forecasting, *ESA Journal, 9*, 125–146.

Wilson, J.W. and Schreiber, W.E. 1986. Initiation of convective storms at radar-observed boundary-layer convergence lines. *Mon. Weath Rev., 114*, 2516–36.